Stress-Strain Properties of Cross Laminated Timber in Compression

Zachary R. Duskin

Alia Amer, Dr. James Ricles, Dr. Richard Sause

Lehigh University

ATLSS

Abstract:

Cross-Laminated Timber (CLT) is created by laminating timber boards together with alternating grain directions. Previous tests have been done to determine the material properties of CLT. However, a more accurate representation of CLT is needed to determine its response under bilateral loads, such as earthquakes. In the study described in this paper, instrumentation was set up to more accurately measure the response of CLT specimens under a compressive load. The results of compression testing are detailed in this paper.

Introduction:

Cross-Laminated Timber (CLT) is created by laminating timber boards together with alternating grain directions, as shown in Fig.1. CLT walls are an innovative way to compensate for timber's material weaknesses. Wood has much more compressive strength parallel the grain than perpendicular to the grain. By alternating the grain patterns, CLT walls provide strength in two directions. CLT walls are growing in popularity as a lateral load resisting material in Europe and some areas of the US (Karacebeyli et al. 2013). However, CLT shear walls are not used in areas with high seismic activity, or in high-rise buildings. Experiments have been conducted to better understand the seismic performance CLT shear walls (Ganey et al. 2015). Previous tests have been conducted on CLT walls that are conventionally connected to floor diaphragms (Dujic et al. 2008).

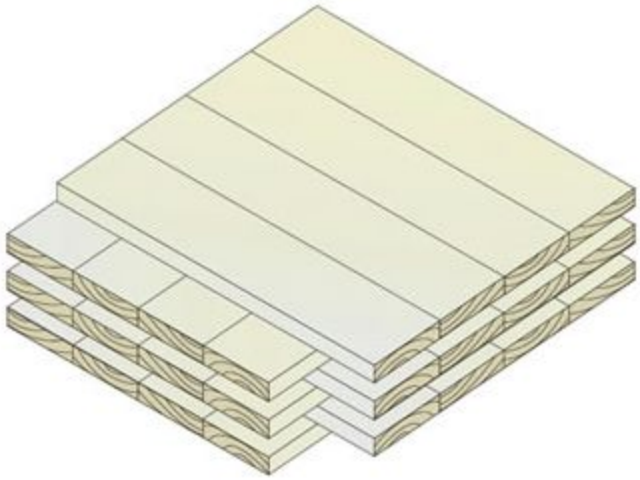

Figure 1: Illustration of Cross Laminated Timber (Karacebeyli et al. 2013).

Earthquake simulations show that CLT walls are capable of resisting severe earthquake forces, but will sustain some structural damage (Ceccotti et al. 2006). A seismically resilient structural system for tall wood buildings can be achieved by using self-centering cross laminated timber (SC-CLT) walls.. CLT walls have been tested with unidirectional lateral loads (Tugce et al. 2017). However, CLT walls have not had adequate testing with bidirectional loads.

Not enough is known about the behavior of CLT walls under high seismic conditions. Models of CLT have been created considering the composite material properties of CLT (Ganey et al. 2015, Akbas et al. 2017). However, under bidirectional lateral loads, CLT wall panels cannot be considered as an isotropic, uniform material. The study described in this paper aims to create data that can be used to create more accurate SC-CLT wall models in order to predict the behavior of SC-CLT in tall buildings without the need for lab testing.

Materials & Instrumentation

Five cross laminated timber specimens, measuring approximately 6.875” by 6.875” by 20.625”, were created for material properties testing under compression.

Linear potentiometers (shown in Fig.2) were used to measure the deformation of the specimens along a gauge length. The potentiometers were calibrated by measuring the output voltage corresponding to being compressed at $\frac{1}{10}$” intervals.The excitation voltage was five volts, and the initial output voltage was five volts. The plunger on the potentiometer was

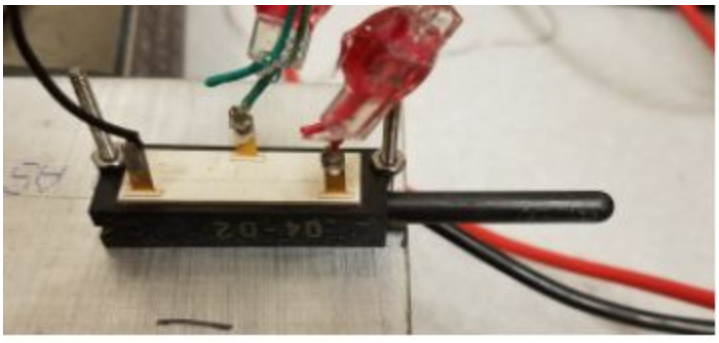

Figure 2: Linear Potentiometer

then compressed using gauge blocks, as shown in Fig.3, and the amount of voltage reduction was recorded. A coefficient corresponding to the ratio of inward motion of the plunge vs. voltage loss for each potentiometer was created using linear regression. The deflection measured by the potentiometers during testing could then be determined by multiplying the coefficient with the voltage value from the potentiometer. When calibrating the plastic sliders, the voltages corresponding to the plunge being fully extended and fully compressed were not considered.

Figure 3: Potentiometer during calibration, with plunger compressed with gauge block

The potentiometers were attached to aluminium plates, shown in Fig.4, which were then mounted onto the specimen. The potentiometers were arranged to measure the deflection of the specimen along its height at three equal length of 6.875". Strain gauges were epoxied to the center of each face of the specimen to measure the strain in the elastic response region. The aluminium plates were mounted on specimen 1 with ¼" threaded rods (shown in Fig.5) that were drilled

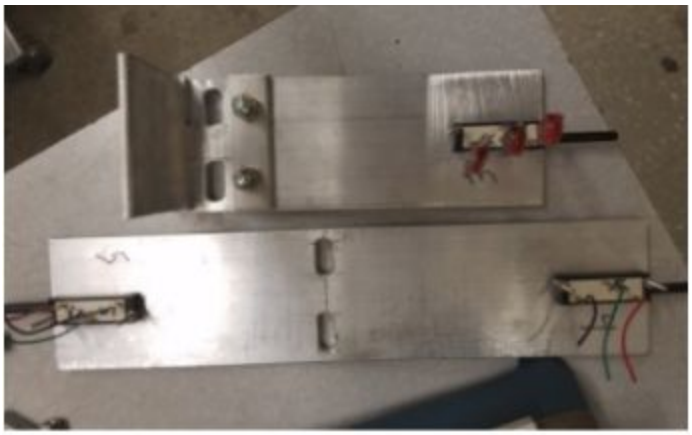

Figure 4: Potentiometers mounted onto aluminium plates.

through the entire thickness of the specimen. The plates were mounted on specimens 2, 3, 4, and 5 using ¼" screws (shown in Fig.5). Each screw penetrated 1 ½" into the specimen.

Figure 6a shows an illustration of the setup of specimen 1, while Fig.6b shows an illustration of specimens 2, 3, 4, and 5. Figures 7a and 7b show the plate and potentiometer set-up on an actual specimen. The plates and potentiometers were placed on the unmilled sides of specimen 1 (shown in Fig. 7a) while the plates and potentiometers were placed on the milled sides of specimen 2 through 5 (shown in Fig.7b).

Figure 5: Threaded rods used on specimen 1 (top)

and screws used for specimen 2-5 (bottom).

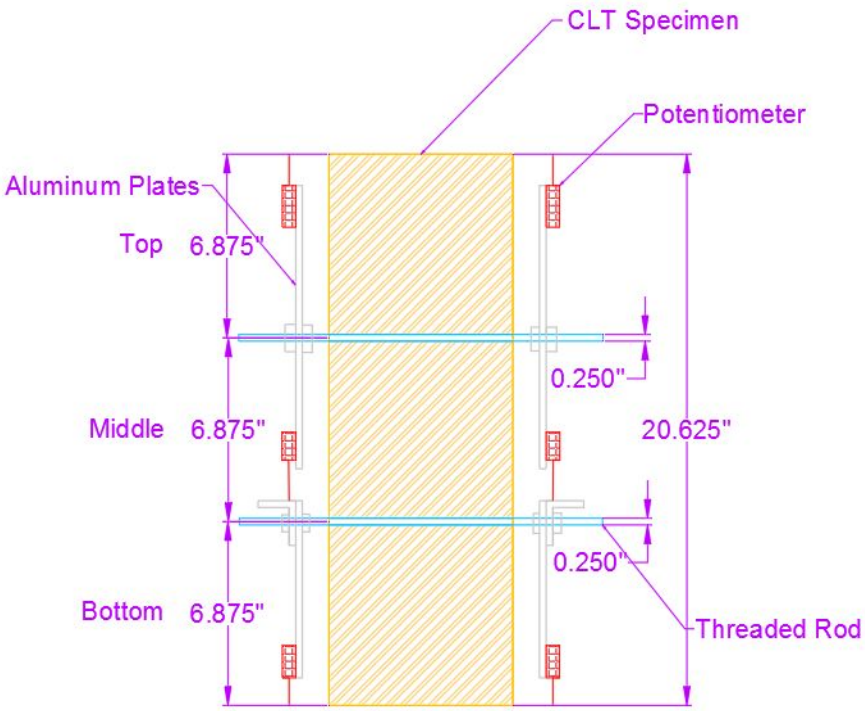

Figure 6a: Specimen 1 set-up.

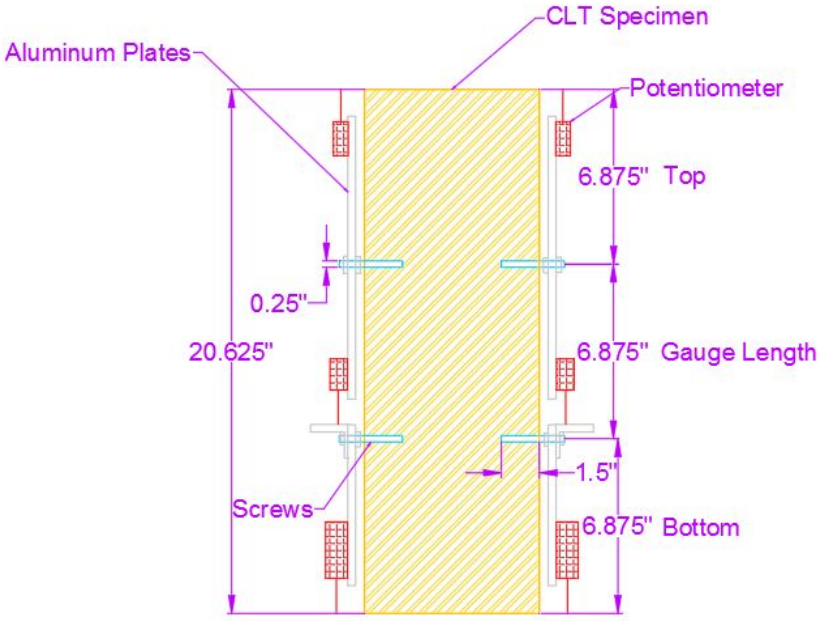

Figure 6b: Specimen 2-5 set-up.

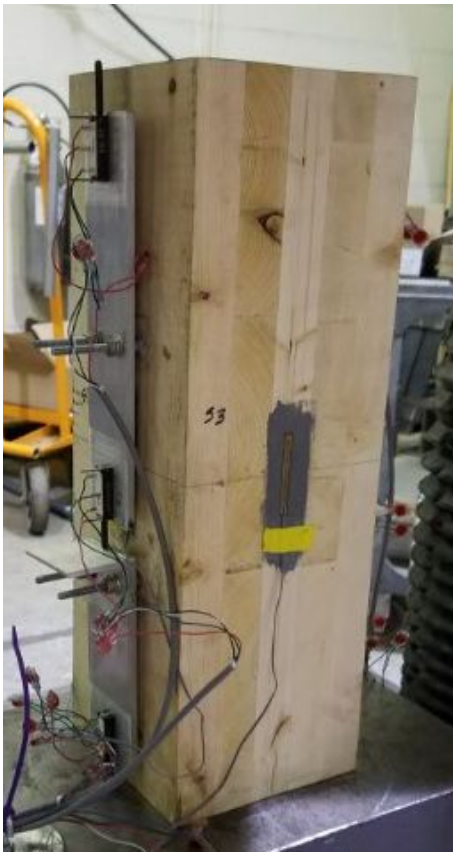

Figure 7a: Aluminium plate and potentiometer set-up for specimen 1.

Figure 7b: Aluminium plate and potentiometer set-up for specimens 2-5.

Methods:

Previous tests have been done to determine the material properties of CLT by comparing an applied load to the deformation of an entire CLT specimen (Ganey et al. 2015). The material properties testing conducted on the CLT specimens discussed in this paper differ aiming to pinpoint the failure of a CLT specimen. Since strain is measured by dividing the change in length of a material by the original length, the stress-strain curve can differ depending on what the original length is considered to be. From observations of Ganey et al. 2015, SC-CLT wall specimens failure, the failure of the wall from rocking is limited to 2.5 to 3 times the thickness of the wall, which is called the characteristic length of failure. The characteristic length of failure is used to create more accurate CLT models.

The height of the specimens was chosen based on the characteristic length of failure found in Ganey et al. 2015 tests. The dimensions of the specimens were 6.875" x 6.875" x 20.625", which satisfy ASTM D4761-13. ASTM D4761 - 13 states that the length of the test specimen shall be at least 2.5 times the length of its greater cross-sectional dimension, and its slenderness ratio (length to least radius of gyration, L/r) of less than 17 to avoid buckling of the specimen. Two pairs of gauge points were chosen according to ASTM D198 - 15 dividing the specimen length over three equal lengths of 6.875".

Several measurements of the specimen's cross-sectional dimensions along its length were obtained using a caliper. Figure 8a shows a typical top view of a specimen, with the unmilled sides labelled "L" and "R," while the milled sides are labelled "T" and "B." Figure 8b shows where the specimen's cross-sectional dimensions were measured along its length.

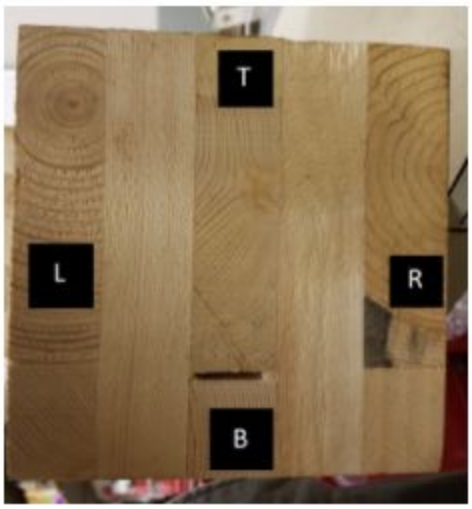

Figure 8a: Top of Specimen with labeled sides.

Sides L and R are unmilled, sides T and B are milled.

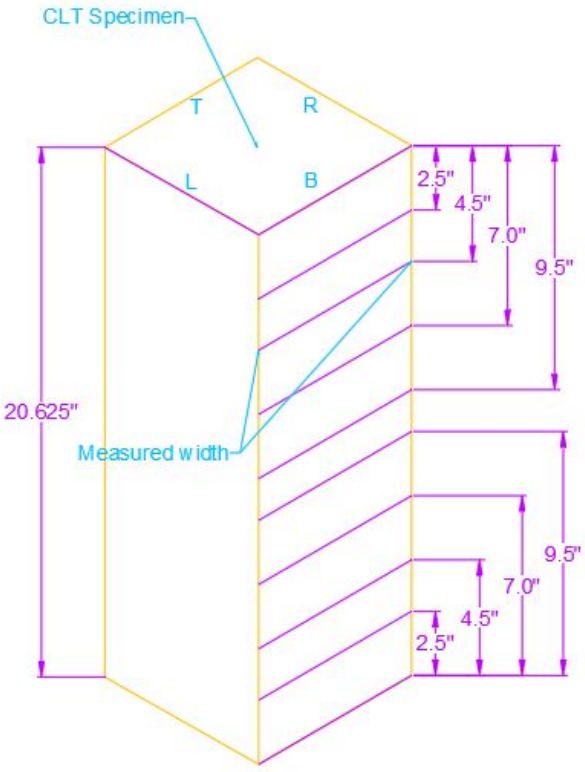

Figure 8b: Width measurements taken along the specimen height

Table 1 shows an example of the measurements collected for each specimen. The stress of each specimen was calculated by dividing the compression load over the corresponding area of the failure zone.

Table 1: Example of Specimen Measurement - Specimen 4

	Width of each specimen side (inches)				Average
	T	B	L	R	Area (in2)
Top of Specimen	6.772	6.795	6.899	6.906	46.82
2.5" down from top	6.8	6.822	6.91	6.916	47.08
4.5" down from top	6.825	6.841	6.902	6.912	47.20
7" down from top	6.83	6.833	6.907	6.909	47.19
9.5" down from top	6.84	6.835	6.904	6.915	47.24
9.5" up from bottom	6.853	6.83	6.909	6.921	47.31
7" up from bottom	6.845	6.814	6.913	6.91	47.20
4.5" up from bottom	6.864	6.811	6.917	6.914	47.28
2.5" up from bottom	6.86	6.809	6.912	6.908	47.23
bottom of specimen	6.848	6.805	6.905	6.913	47.16

The CLT specimens were tested in compression using a SATEC universal testing machine. Each test began in force control, in which the SATEC applied load at a given rate until a certain percentage of the specimen's estimated peak load was reached.

Afterwards, the SATEC switched to displacement control. The rate of loading was similar to the force control stage, however, in displacement control the SATEC would not attempt to keep increasing the load after the peak stress, defined as the "yield "stress, was reached. The CLT compressive stress decreases after reaching the yield stress, and so the SATEC attempting to reach higher stress levels would result in the specimen being crushed suddenly.

Finally, at a predetermined point after the yield strength was reached, the SATEC switched to a faster displacement control rate. The final loading rate was faster to decrease the testing time. The loading rates were in accordance with ASTM D4761-13, which specifies that ,

when testing structural wood in compression, the yield load shall not be reached before four minutes.

Table 2 shows the load rates and switching points for each stage for all specimens. Figure 9 shows an example of a Force vs. Displacement graph divided into the three testing phases.

Table 2: Testing procedure rates for each specimen.

Test procedure	*Specimen 1*	*Specimen 2*	*Specimen 3, 4, & 5*
Force Control (kip/min)	10	12	12
Up to (kips)	40	24	24
Displacement Control (in/min)	0.01	0.01	0.01
Up to (in.)	0.3	0.45	0.6
Displacement Control (in/min)	0.05	0.04	0.02
Up to (in.)	1	failure	failure

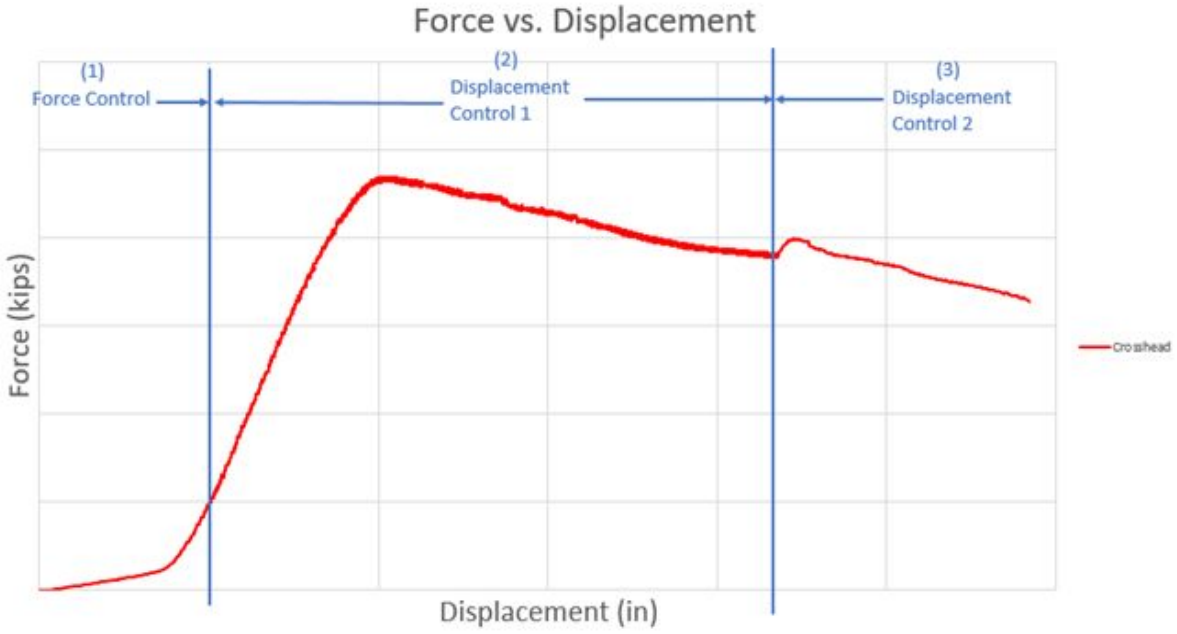

Figure 9: Example of the three testing phases on a Force vs. Displacement plot of specimen 2.

Results:

Specimen 1:

Figure 10 shows specimen 1 after compression testing. Specimen failure occurred at the cross section where the bolts were inserted. The specimen deformed unevenly, resulting in specimen bending.

The aluminium plates were mounted on threaded rods that were drilled into the unmilled side of the specimen, which caused some initial damage to the specimen.

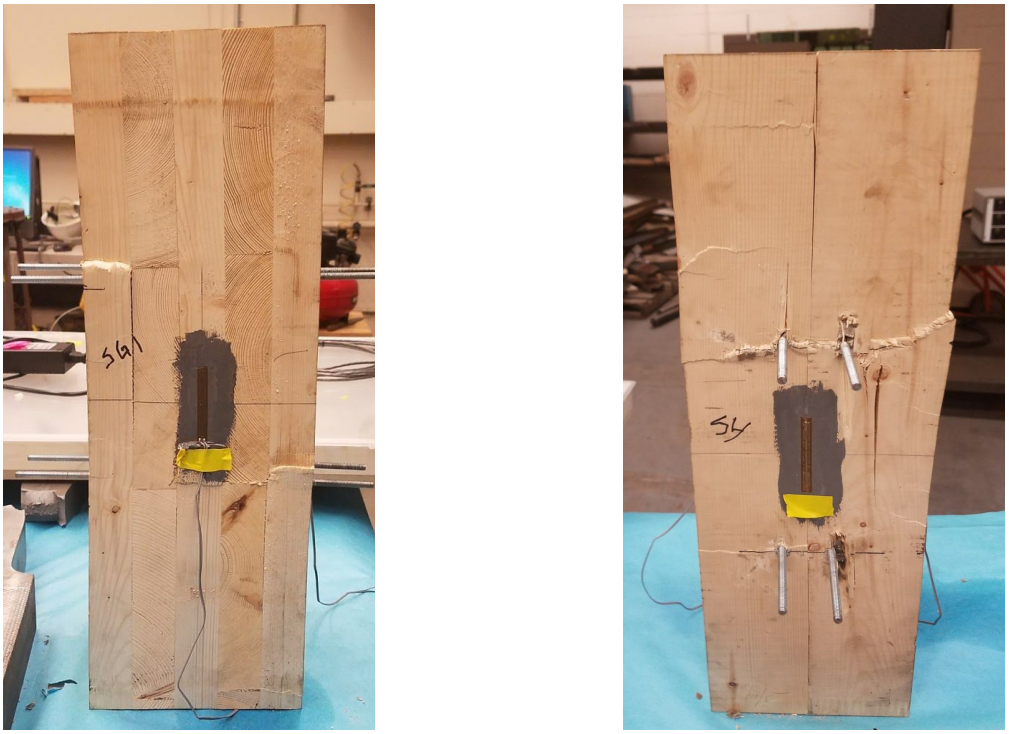

Fig 10: Specimen 1 After Failure.

Specimen 2:

Specimen 2 experienced failure along the middle gauge length, seen in Fig.11. The stress-strain response of the strain gauges, the potentiometers, and the force-displacement plot for specimen 2 are shown in Figs. 12, 13, and 14, respectively. Stress was found by dividing the applied load by the cross sectional area of the failure zone. An upwards bump can be seen in the Fig.13 and Fig.14 where the second displacement load rate began. The bump was caused by the sudden load rate increase, which caused the specimen to appear stronger for a short time. The load rate was not increased as sharply on future specimens.

The crosshead displacement increases at a faster rate initially, due to some slack in the testing machine. After the initial slack is taken out, the slope of the crosshead's stress-strain and force-displacement response mimics the slope of the potentiometer's responses.

The aluminium plates were mounted onto specimen 2 using screws, which penetrated into the specimen's unmilled side. The screws were inserted into the sections of the specimen with the wood grain running horizontally. Drilling the screws parallel with the wood grain resulted in less damage than previously caused on specimen 1 with the threaded rods.

The strain along the upper, middle, and lower gauge lengths are represented in each specimen's stress-strain and force-deflection plots by the lines "1&4," "2&5," and "3&6," respectively. The deformation in each section was calculated by averaging the deflection of the two corresponding potentiometers (e.g. averaging potentiometer 1 and 4 to find deformation of top section). The deformation was converted to strain by dividing the average deflection of each section by its corresponding length.

The stress-strain response of potentiometers 2 and 5 show much more strain after yielding than potentiometers 1&4, and 3&6, which is in good agreement with the appearance of specimen 2's failure location.

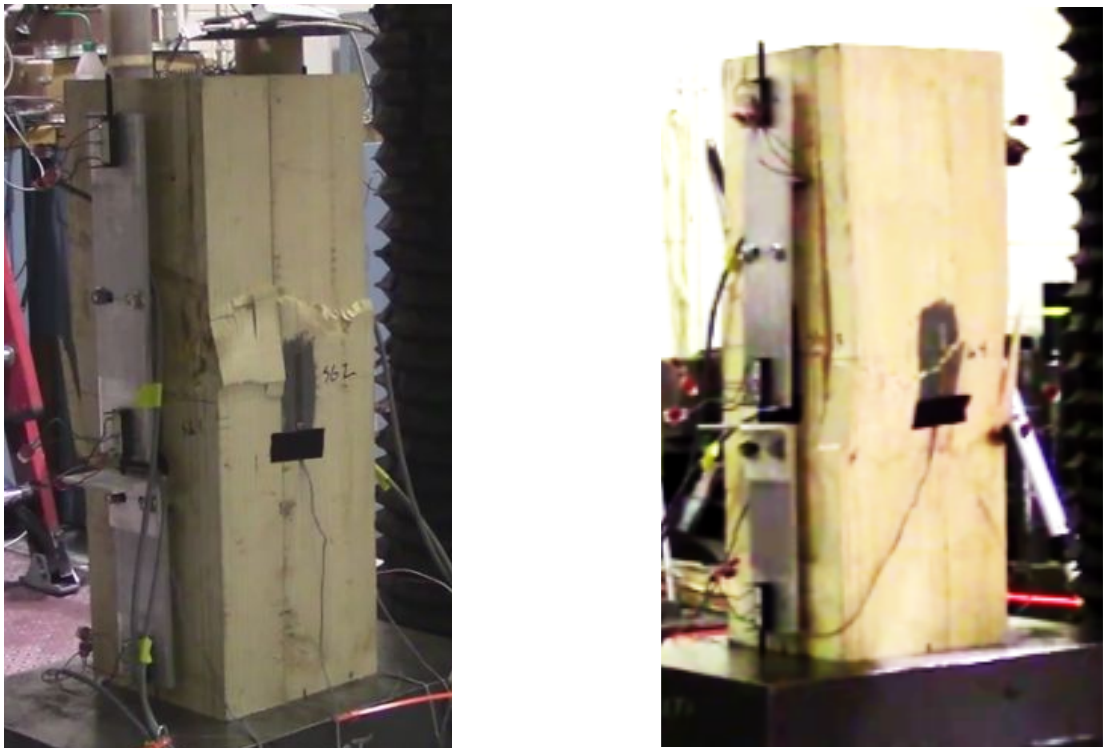

Figure 11: Specimen 2 after failure

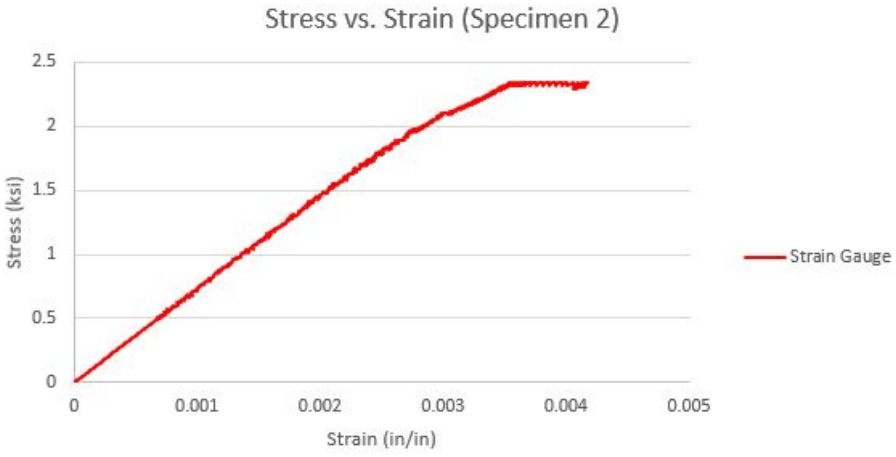

Figure 12: Stress-strain response of strain gauges for specimen 2.

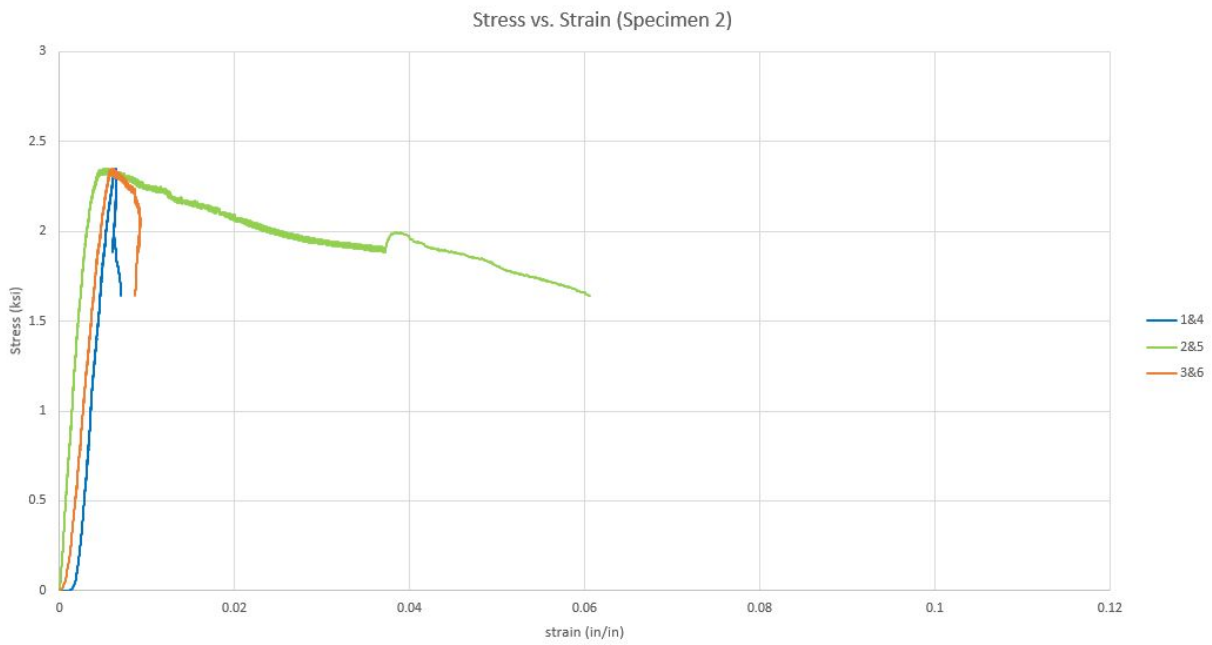

Figure 13: Stress-strain response of specimen 2 from potentiometers.

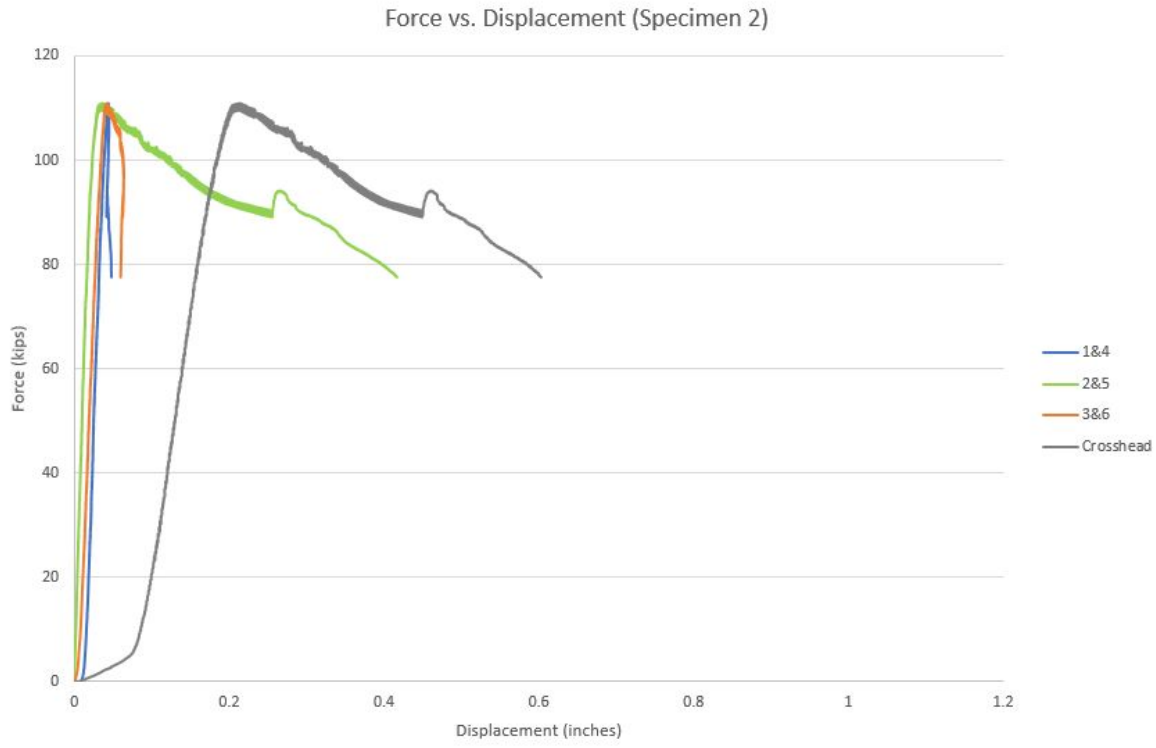

Figure 14: Force-deformation readings of potentiometers and crosshead for specimen 2.

Specimen 3:

Specimen 3 failed in the upper gauge length, shown in Fig.15. Figures 16 and 17, show the stress-strain response of the strain gauges and the potentiometers, respectively. The potentiometer response also indicates the specimen failure occurring in the upper section along potentiometers 1 and 4.

Figure 18 shows the force-displacement response of the specimen. The bumps between the two displacement control testing stages in Figs.17 and 18 are not as prominent as the ones seen in specimen 2's stress-strain and force-displacement graphs (Figs.13 and 14).

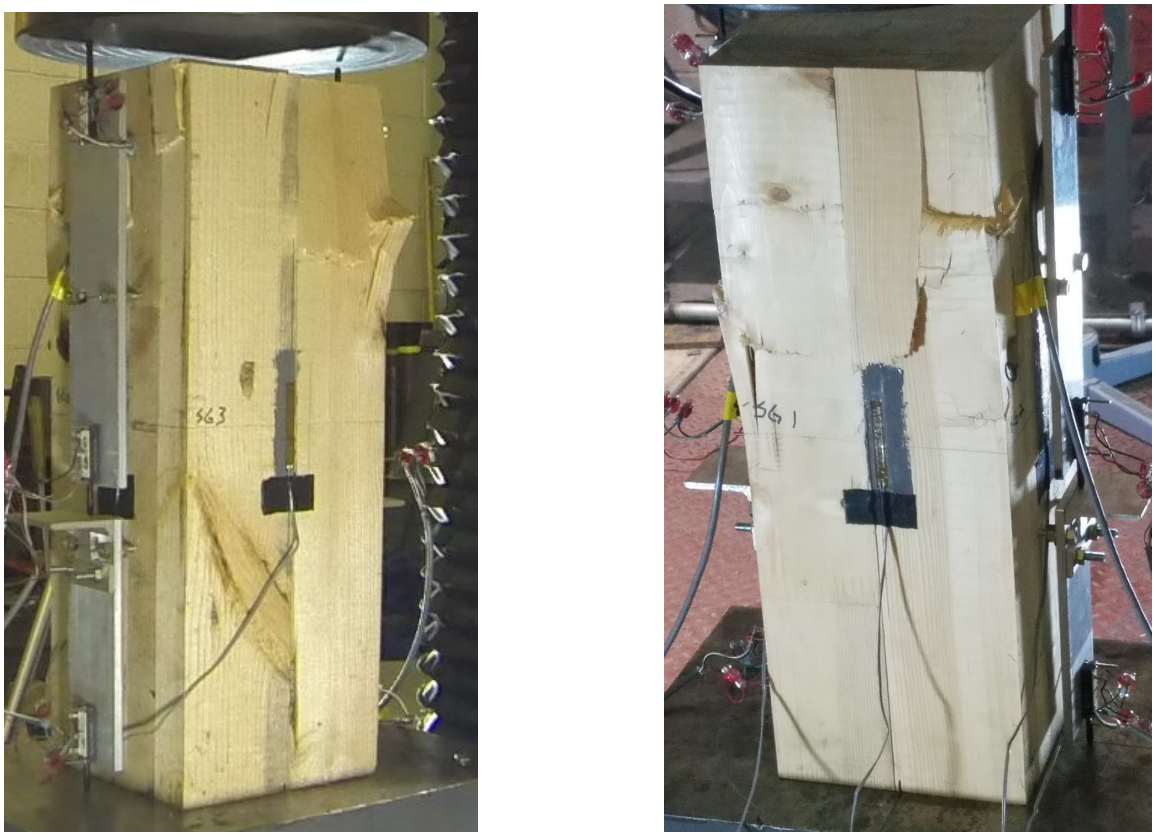

Figure 15: Specimen 3 failure

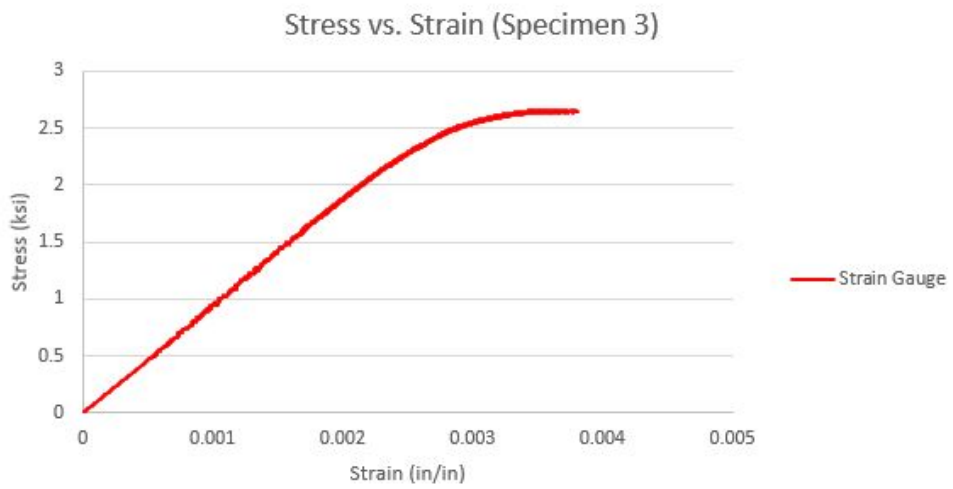

Fig 16: Stress-strain response of strain gauges for specimen 3.

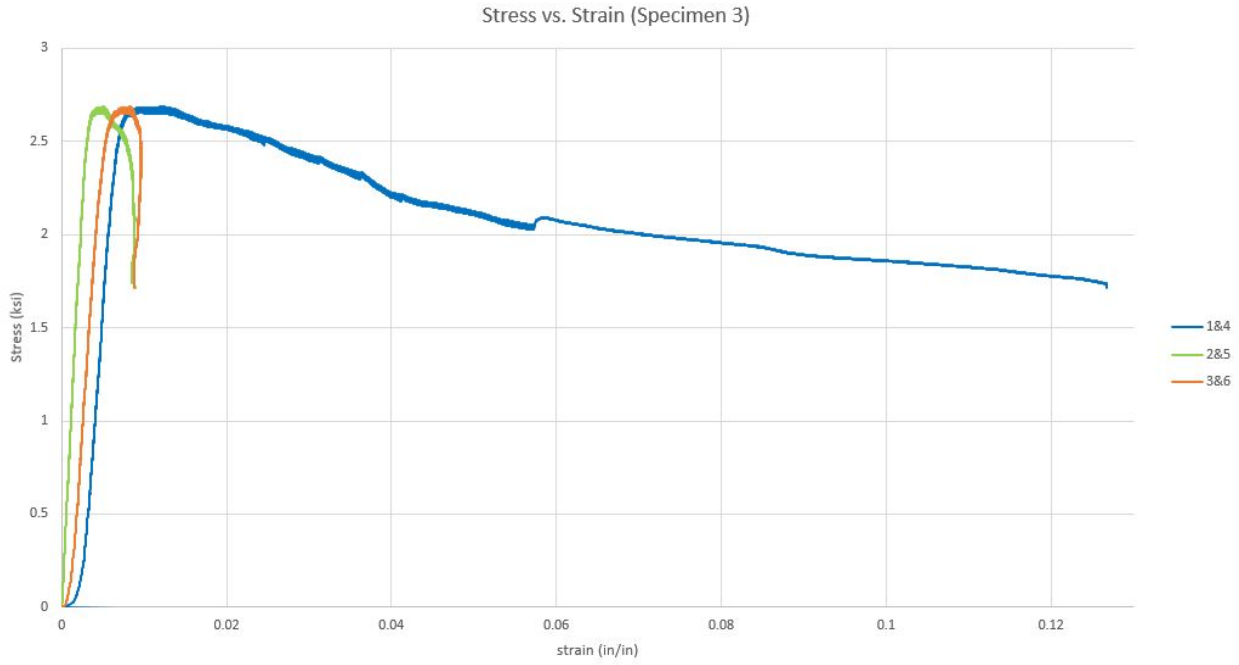

Figure 17: Stress-strain response of specimen 3 from potentiometers.

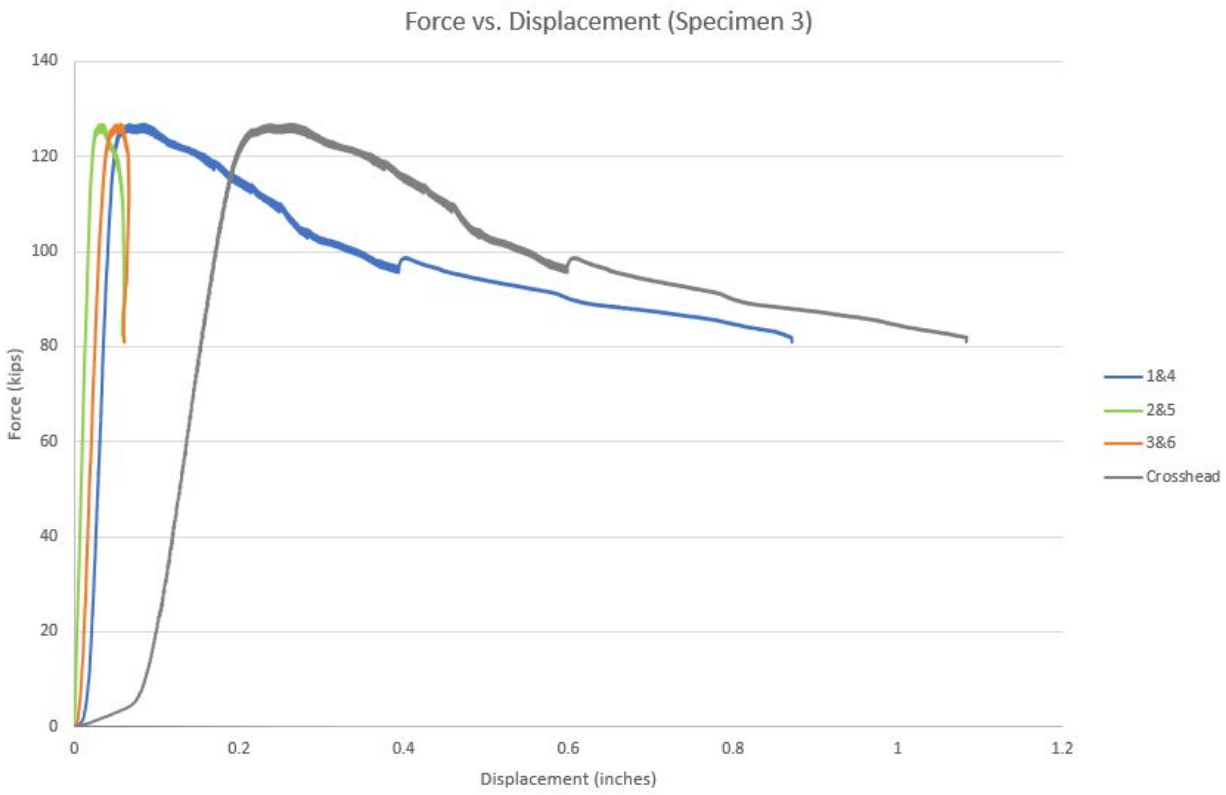

Figure 18: Force-deformation readings of potentiometers and crosshead for specimen 3.

Specimen 4:

Specimen 4 failed in the upper gauge length, shown in Fig.19. Several holes about 1mm in diameter were found the unmilled sides of specimen 4 before testing. Specimen damage occurred along the small holes.

Figures 20 and 21 show the stress-strain response of the strain gauges and the potentiometers for specimen 4, respectively. Figure 22 shows the force-displacement plot for specimen 4.

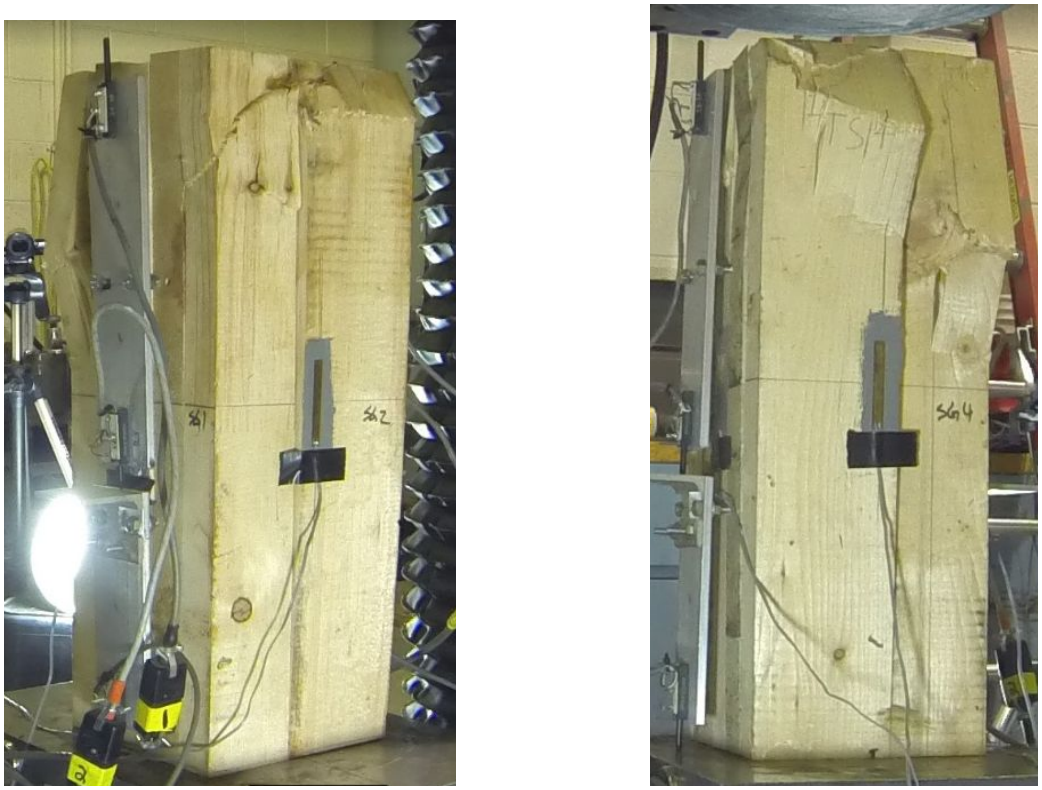

Figure 19: Specimen 4 failure

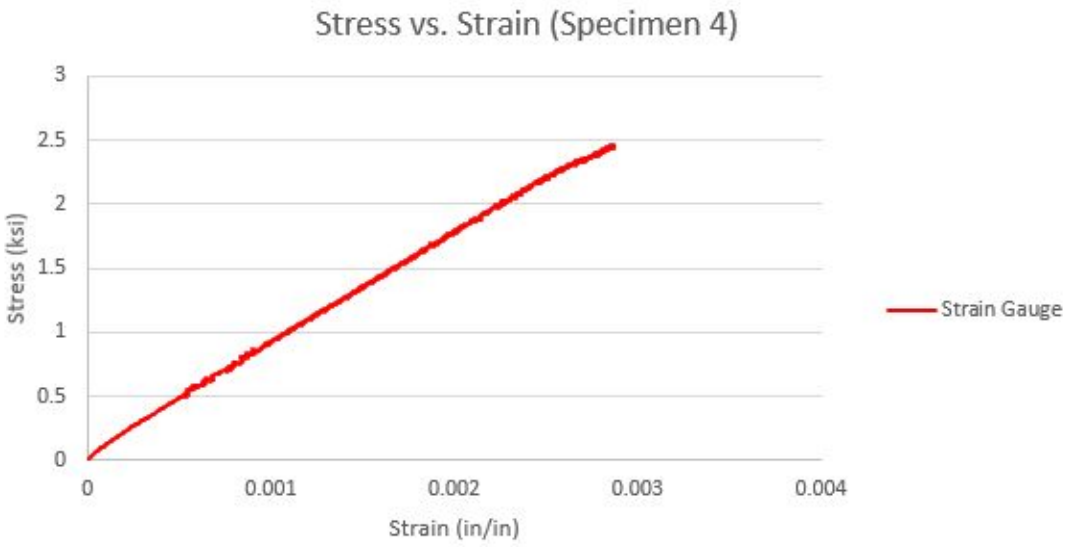

Figure 20: Stress-strain response of strain gauges for specimen 4.

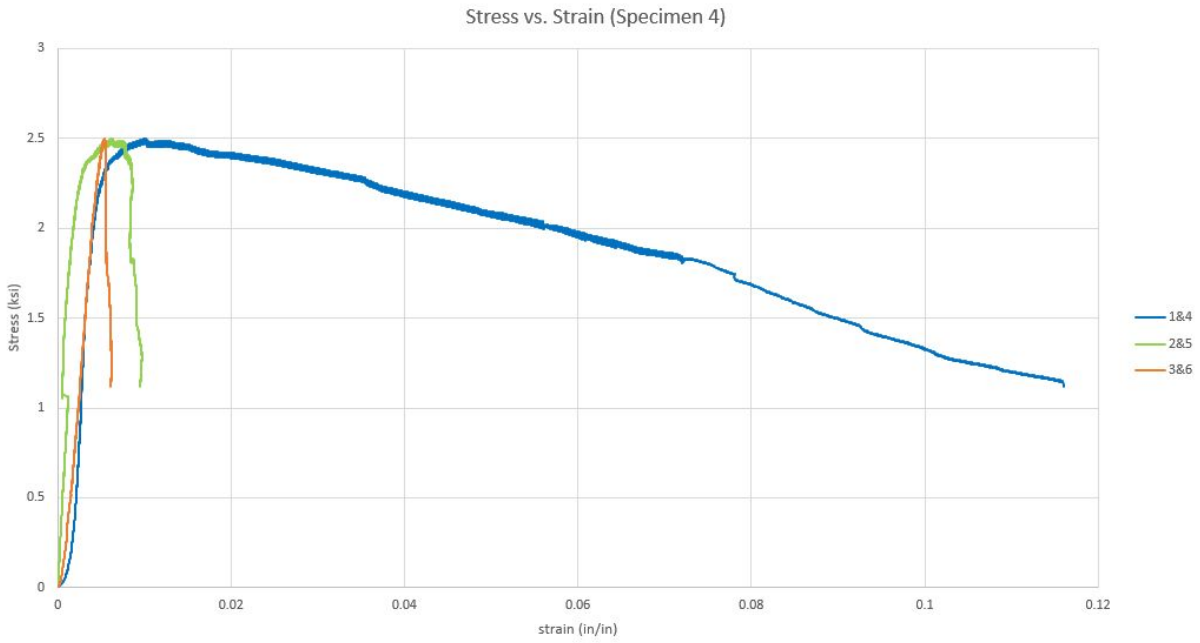

Figure 21: Stress-strain response of specimen 4, according to potentiometers.

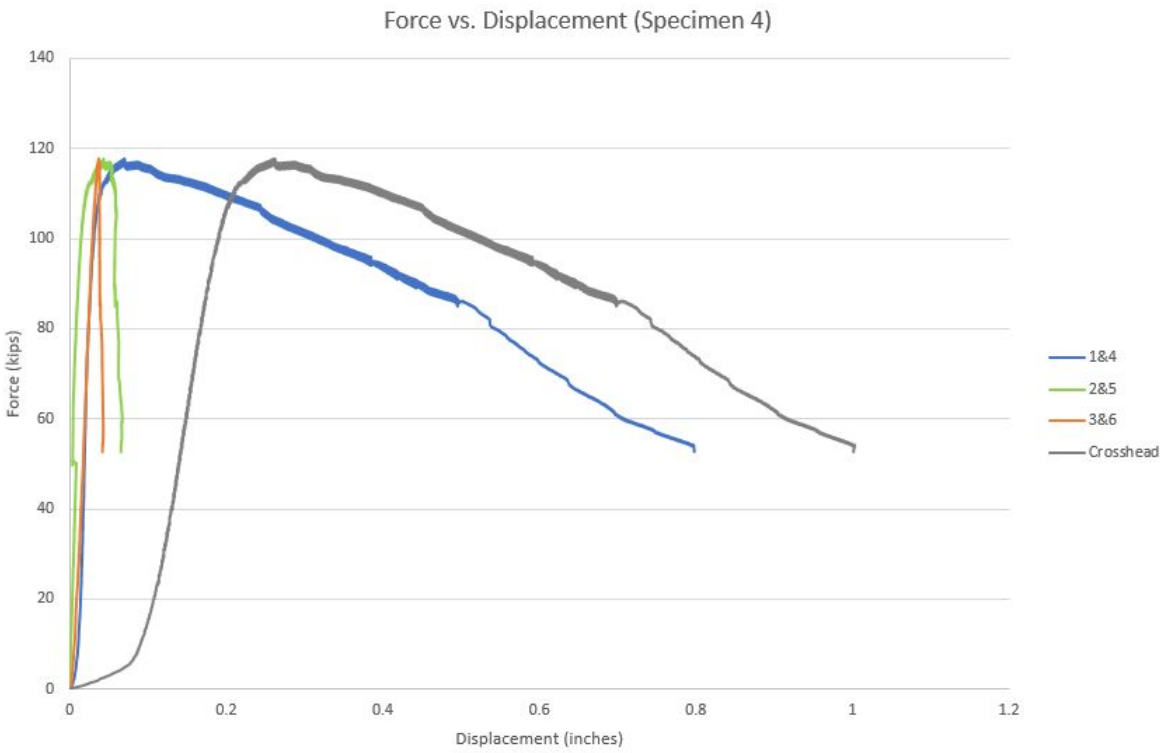

Figure 22: Force-deformation readings of potentiometers and crosshead for specimen 4.

Specimen 5:

Specimen 5 failed in the lower and middle gauge lengths, shown in Fig.23.

A small section of wood split from the specimen while loading. The area under strain gauge 4 was damaged (seen in Fig.23, left) so strain gauge 4's readings were not considered when calculating the specimen's stress-strain response.

Figures 24 and 25 show the stress-strain response of the strain gauges and the potentiometers for specimen 4, respectively. Figure 26 shows the force-displacement plot for specimen 4.

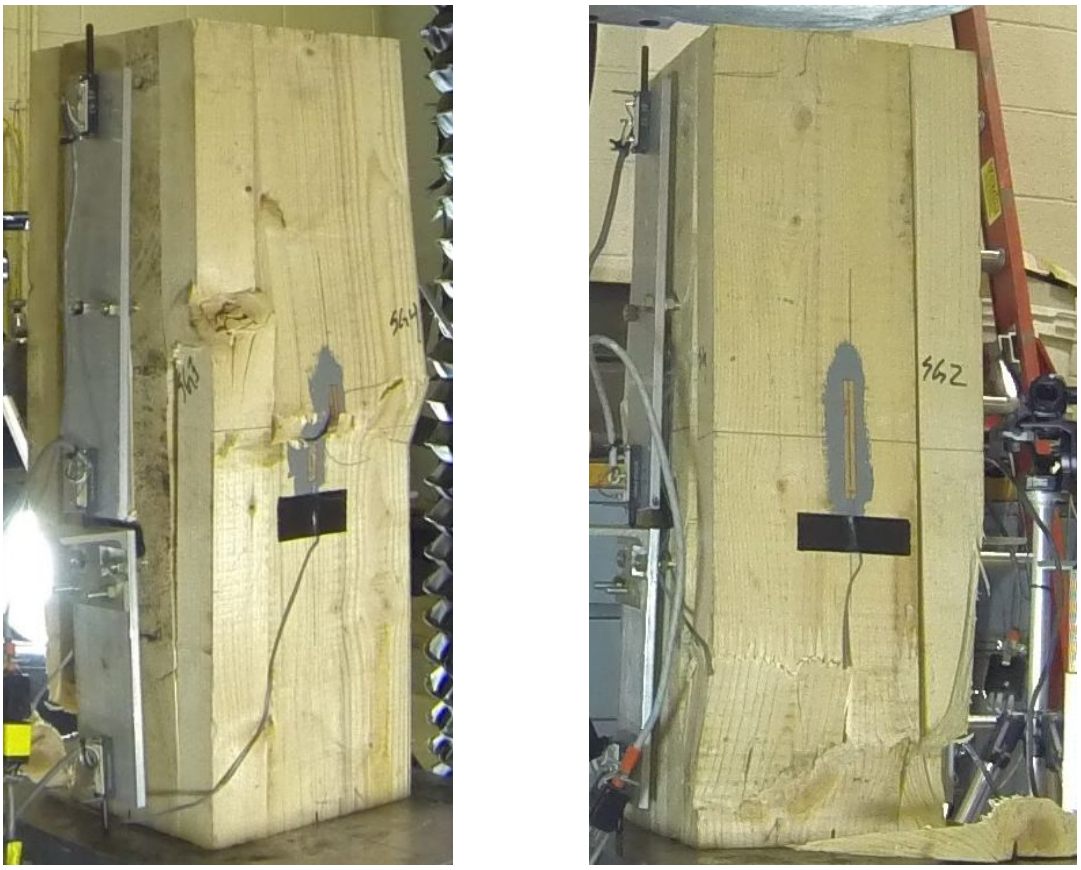

Figure 23: Specimen 5 failure

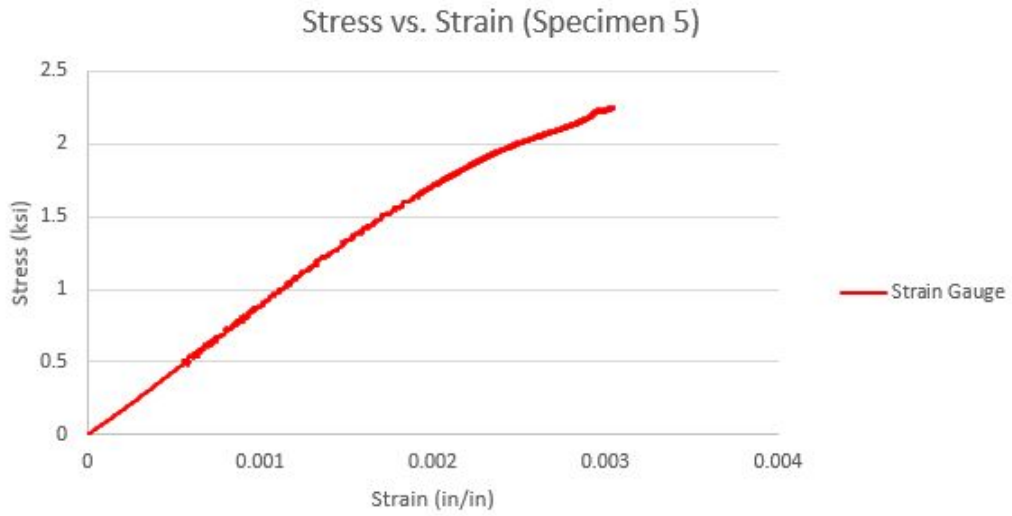

Figure 24 : Stress-strain response of strain gauges for specimen 5

Figure 25: Stress-strain response of specimen 5, according to potentiometers.

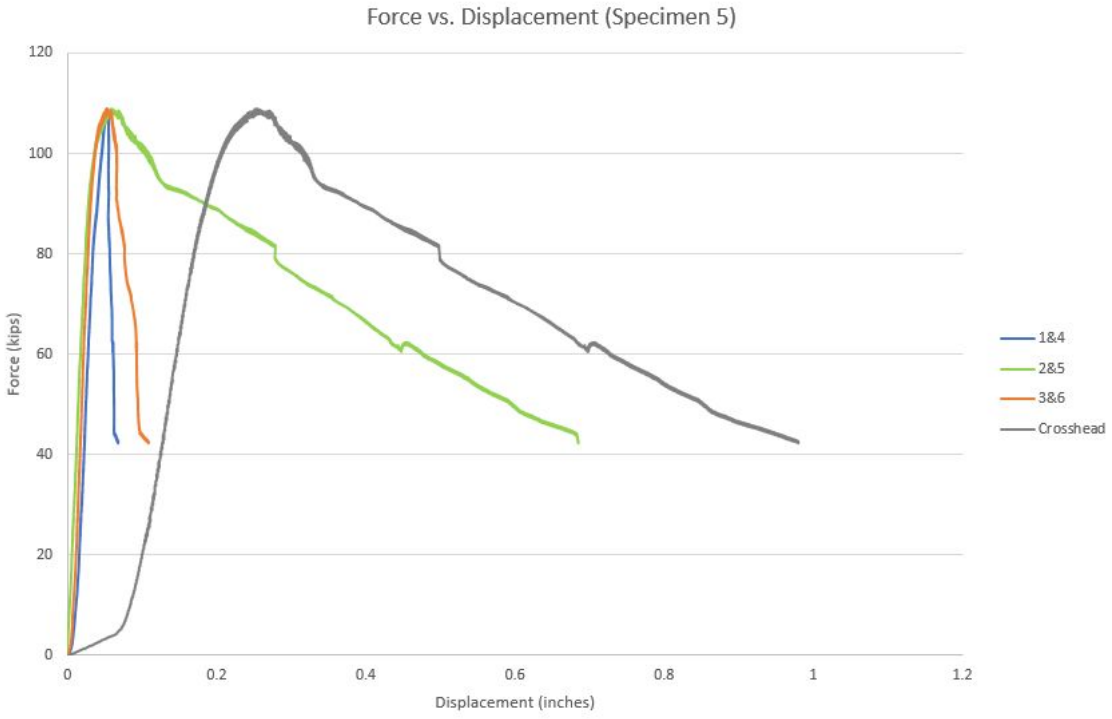

Figure 26: Force-deformation readings of potentiometers and crosshead for specimen 5.

Discussion:

The failure pattern of specimen 1 shown in Fig.10 suggests that the specimen may have failed prematurely due to the rods running through the thickness of the entire specimen. The specimen experienced failure along the cross section where the rods were inserted, as seen in Fig.10. The rods were inserted perpendicular to the the grain of the individual boards, which caused premature separation of the wood fibers. Also, the bending of the specimen was most likely caused by using a spherical bearing on the crosshead, which allowed the crosshead to rotate. The test results for specimen 1 were not plotted, since the results were not believed to be reflective of the specimen's true properties.

Specimen 2 failed along the middle gauge length. The stress-strain response of the strain gauges are in good agreement with the stress-strain measurements from potentiometers 2 and 5. The potentiometers were attached to following specimens using screws instead, to minimize the risk of pre-induced failure. Additionally, the screws were inserted parallel to the grain of the individual boards, which minimized damage before testing. A large jump in the data can be seen in Figs. 13 and 14 where the third testing phase begins, due to the change in testing speed. Specimens 3, 4, and 5 were tested with a slower third testing phase in order to minimize the data jump.

Specimen 3 failed in the upper section of the specimen. It was assumed that all of the specimens would most likely fail in the center section, since the upper and lower portions are somewhat restrained from movement by the testing apparatus. However, the results of specimen 3 suggest that failure is possible in the upper and lower sections of the CLT specimens.

The failure pattern of specimen 4 was due to a defect in the specimen. Several small holes approximately 1mm in diameter were found on the unmilled sides of specimen 4. Cracks formed running through the holes, suggesting that the specimen may have failed prematurely because of them. Also, one of the potentiometers on specimen 4 was not in contact with the surface of the crosshead, and so the potentiometer's deformation data is not completely accurate.

Damage can be seen in the bottom section of specimen 5, as seen in Fig.23. However, the test data shows the specimen deformed mostly in the middle section while displaying a strain hardening behavior in the lower section.

Overall, CLT is a highly variable material with regards to total strength. Fig. 27 shows the stress-strain data of the failure zones of specimens 2 through 5.

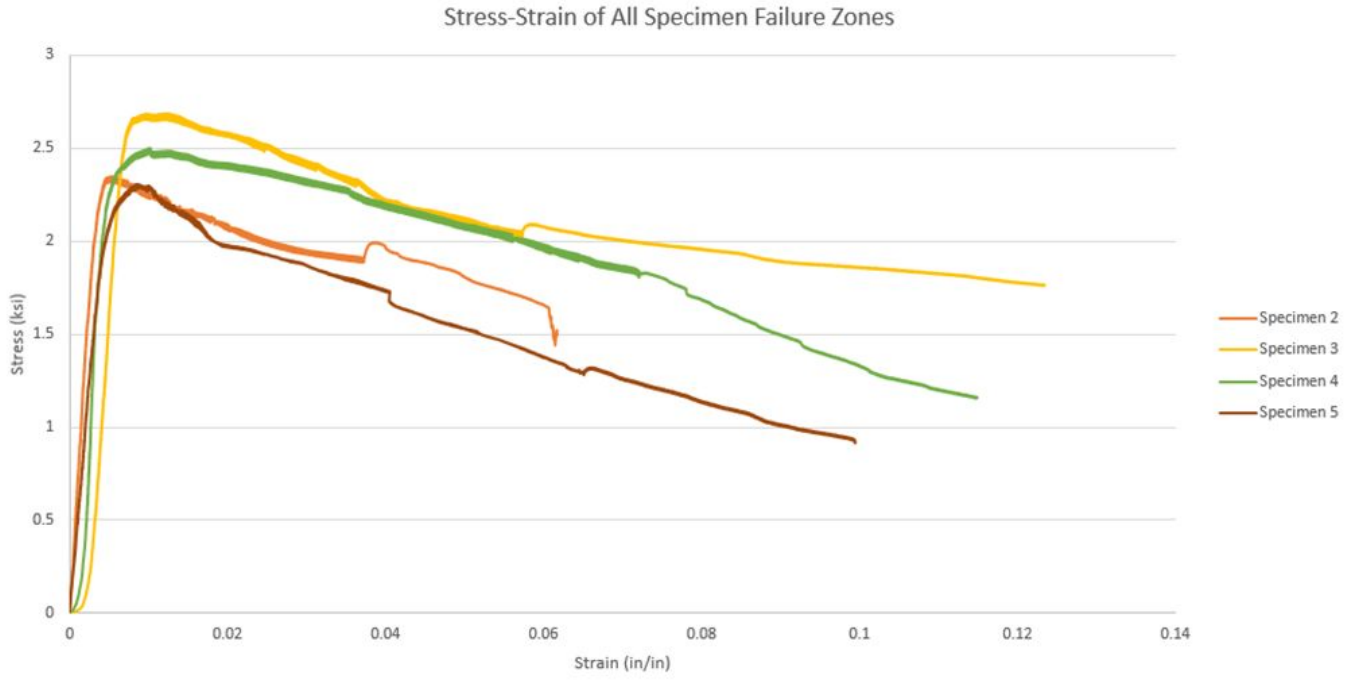

Figure 27: Stress-Strain data of the failure zones of specimens 2-5.

Further research should be done to refine and standardize the CLT specimen testing procedure. The results discussed in this study can contribute to the creation computer-based models in order to predict the behavior of SC-CLT walls.

Acknowledgements:

Alia Amer	Dr. Richard Sause	Dr. James Ricles
Carl Bowman	Peter Bryan	Darrick Fritchman
NHERI	Dr.Karina Vielma-Cumpian	Dr. Chad Kusko

References (ASCE Format):

Akbas, T., Sause, R., Ricles, J. M., Ganey, R., Berman, J., Loftus, S., Dolan, J. D., Pei, S., van de Lindt, John W, and Blomgren, H. (2017). "Analytical and Experimental Lateral-Load Response of Self-Centering Posttensioned CLT Walls." *J.Struct.Eng.,* 143(6), 04017019.

ASTM D4761-13 Standard Test Methods for Mechanical Properties of Lumber and Wood-Base Structural Material, ASTM International, West Conshohocken, PA, 2013, https://doi.org/10.1520/D4761-13

Ceccotti, A., Lauriola, M. P., Pinna, M., and Sandhaas, C. (2006). "SOFIE project–cyclic tests on cross-laminated wooden panels." *proceedings of the 9th world conference on timber engineering, Portland, Oregon, USA,* .

Dujic, B., Klobcar, S., and Zarnic, R. (2008). "Shear capacity of cross-laminated wooden walls." *Proceedings of the 10th World Conference on Timber Engineering, Miyazaki, Japan,* .

Ganey, R. S. (2015). *Seismic Design and Testing of Rocking Cross Laminated Timber Walls,* .

Karacebeyli, E., and Douglas, B. (2013). "CLT Handbook-US Edition." *Library and Archives Canada Cataloguing in Publication, Quebec, Canada,* .